

Cell Sorting in Three Dimensions: Topology, Fluctuations, and Fluidlike Instabilities

M. Shane Hutson,^{1,*} G. Wayne Brodland,^{2,3,*} Justina Yang,² and Denis Viers²

¹*Departments of Physics & Astronomy, Biological Sciences and Vanderbilt Institute for Integrative Biosystem Research & Education, Vanderbilt University, Station B #351807, Nashville, Tennessee 37235, USA*

²*Department of Civil and Environmental Engineering, University of Waterloo, Waterloo, Ontario N2L 3G1, Canada*

³*Department of Biology, University of Waterloo, Waterloo, Ontario N2L 3G1, Canada*

(Received 3 June 2008; published 3 October 2008)

Previous 2D and 3D models concluded that cell sorting requires cytoskeletal fluctuations and is stalled by high tension at heterotypic interfaces. New deterministic and stochastic models show that this is not true in 3D. Sorting in 3D involves both topological untangling and domain coalescence. Coalescence requires fluctuations and low tension, but untangling does not. It occurs by a Plateau-Rayleigh instability of cell threads—deterministically driven by high tension. At high minority-cell fractions, untangling dominates and significant partial sorting can occur without fluctuations.

DOI: [10.1103/PhysRevLett.101.148105](https://doi.org/10.1103/PhysRevLett.101.148105)

PACS numbers: 87.17.Rt, 02.40.Pc, 47.20.Dr, 87.17.Aa

When two types of suitable embryonic cells are formed into a well-mixed aggregate, the cells will slowly sort into distinct cell-type-specific domains [1–6]. Experimental evidence strongly supports the hypothesis that cell sorting is driven by cell-type-specific surface energies (or interfacial tensions) [7]. The consequences of this hypothesis have been investigated many times, with many different computational models (reviewed in [6]), but almost always in two-dimensions (2D). For sorting of two cell types (light and dark), the basic model parameters are five contact surface energies: two for contact of each cell type with the surrounding medium, γ_{L0} , γ_{D0} ; two for homotypic cell-cell contacts, γ_{LL} , γ_{DD} ; and one for heterotypic contacts, γ_{LD} . Differences among these five energies can be grouped into three macroscopic surface tensions: $\sigma_L = \gamma_{L0} - \gamma_{LL}/2$; $\sigma_D = \gamma_{D0} - \gamma_{DD}/2$; and $\sigma_{LD} = \gamma_{LD} - (\gamma_{LL} + \gamma_{DD})/2$ [8]. These surface tensions determine the lowest energy configuration, e.g., the larger of σ_L and σ_D determines which cell type is more stable in the interior. For complete engulfment, the heterotypic surface tension, σ_{LD} , is then constrained by $\sigma_{D \text{ or } L} > (\sigma_D + \sigma_L - \sigma_{LD})/2 \geq \sigma_{L \text{ or } D}$ [9]. Within this constrained range, higher values of σ_{LD} hinder 2D sorting kinetics—even leading to kinetically trapped cases of incomplete sorting [10].

In a few cases, similar models and their predictions have been successfully extended to three-dimensions (3D) [11–15]; however, the roles of key model parameters in 3D have only been given a cursory examination—generally concluding that the dependence in 3D follows that in 2D [14]. This is certainly true for determining the lowest energy configurations, but not so for determining the sorting kinetics. Here, we present an examination of 3D cell sorting using two different models—a cellular Potts model and a new finite-element model. Results from both show that parameter dependencies established with 2D models cannot be extrapolated to 3D. Such extrapolations overstate the role of active cytoskeletal fluctuations and oversimplify the role of tension at heterotypic interfaces. Although

presented in the context of cell-sorting, these dimensionality differences are relevant to virtually all cell-cell mechanical interactions—including those typically involved in embryogenesis, cancer metastases and tissue engineering.

To understand what is missing from previous accounts, we first examine the topology of unsorted, 3D cell aggregates (Fig. 1). When the fraction of minority cells is low ($f < 0.1$), the minority cells are connected into multiple, isolated small domains—as evidenced by the small number of minority cells in the largest connected domain and by the large positive Euler characteristic (χ). For closed 3D solids, the intuitive definition is $\chi = \#\text{components} - \#\text{holes} + \#\text{cavities}$. In practice, χ is computed by integrat-

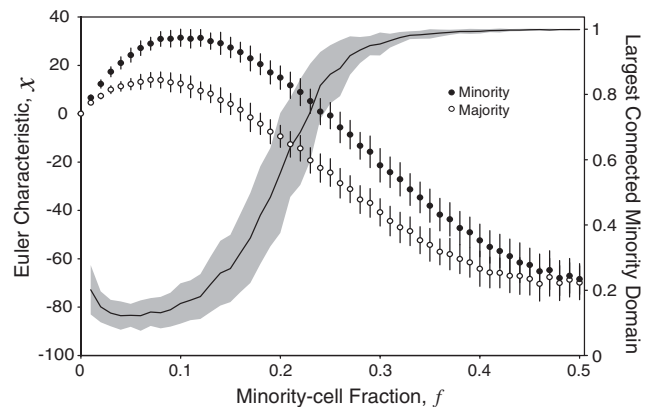


FIG. 1. Topological characteristics of cell-type domains in unsorted 3D aggregates. A 670-cell Voronoi tessellation of a sphere was briefly annealed with a cellular Potts model. Cells were then randomly assigned to one of two types. For each minority cell fraction, the topology was characterized for 100 sets of random cell-type assignments: Euler characteristic of minority cells (filled circles) and majority cells (open circles), and fraction of minority cells in the largest connected domain (solid line). The error bars and shaded region denote 1 standard deviation.

ing curvature over the bounding surfaces and applying the Gauss-Bonnet theorem [16]. The positive χ at low f arises from summing over multiple isolated domains. Each domain has just a few cells and is thus likely to have $\chi = 1$ (no cavities, loops, or tunnels). As the minority-cell fraction increases, the topology changes dramatically. For $f \geq 0.3$, more than 95% of the minority cells are connected to a single domain—easily missed if cells are viewed only in cross section [15]. This large domain now has a large negative Euler characteristic corresponding to a connected structure with dozens of loops and tunnels. Note that the Euler characteristic for the single majority domain is even more negative. Thus, for high minority-cell fractions, the minority- and majority-cell domains are tangled, co-continuous phases.

With different initial topologies, the process of cell sorting has to accomplish quite different tasks. At low f , the primary task is the coalescence of isolated minority domains. At high f , the minority and majority domains must also untangle—which often breaks the minority cells into multiple domains—and then these domains must coalesce. Of course, one cell type must also be excluded from the aggregate surface. In this Letter, we show that the untangling process is what complicates the role of tension at heterotypic interfaces. Untangling also allows significant sorting to take place without cytoskeletal fluctuations.

To model cell sorting without fluctuations, we used a new 3D model based on the finite-element method [6]. Cells in the model are assumed to carry tensions γ along each cell-cell or cell-medium interface. The strength of each γ is specific to the cell type(s) at that interface. These interfacial tensions should not be confused with macroscopic surface tensions, σ . They are instead directly equivalent to the contact surface energies and are a composite of multiple factors: contraction of actin networks and other surface-associated protein systems; membrane contraction; and an equivalent in-plane force produced by cell-cell adhesion [5,17,18]. Each cell is filled with a fluid having an effective viscosity μ that arises from the deformability of the cytoplasm and its embedded networks [6,17]. At each time step, the model balances the applied and viscous forces at each vertex to deterministically solve for the next set of vertex displacements. Iterative solutions allow the cells to move. In addition, cells can gain or lose neighbors via an appropriate rearrangement algorithm [11,19].

An example of cell sorting with this model is shown in Fig. 2 (and Movie 1, see supplementary material [20]). The initial configuration is slightly atypical ($\chi_D = -1$ is too low), but was chosen for its illustrative value. The ratio of interfacial tensions was chosen so that the heterotypic tension, γ_{LD} , was near the high end of its constrained range ($\gamma_{LL}:\gamma_{DD}:\gamma_{LD}:\gamma_{L0}:\gamma_{D0} = 1:1:4:2:6$ which yields $\sigma_L:\sigma_{LD}:\sigma_D = 3:6:11$). As the simulation runs, this strong tension smoothes heterotypic interfaces and causes the branchlike projections to shorten and thicken. These actions are similar to 2D simulations [6,17], but the behavior

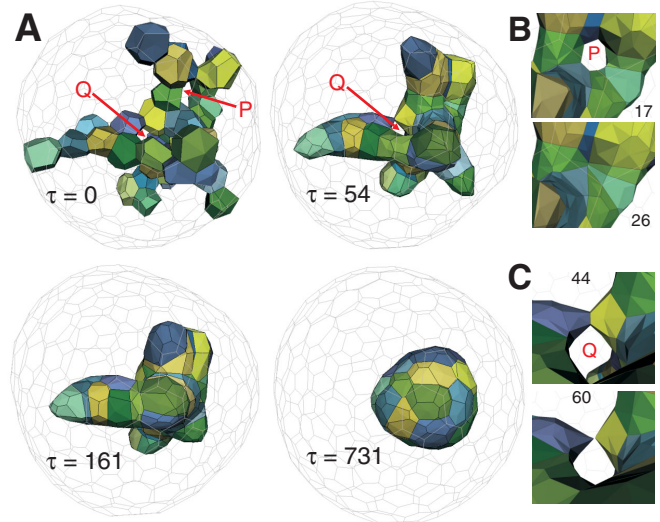


FIG. 2 (color online). Finite-element simulation of 3D cell sorting. The pseudorandom initial configuration of 454 cells has all 36 minority cells in one connected domain. (a) Cell configurations at the labeled times during sorting. For clarity, the majority cells are only indicated by thin gray outlines. Arrows **P** and **Q** indicate loops created by multiply connected chains of minority cells. (b) Close-up view as the loop indicated by **P** seals off—breaking the bridge of majority cells that connected through its lumen. (c) Close-up view as the loop indicated by **Q** opens by breaking a chain of minority cells. Reported times are dimensionless and defined as $\tau = \frac{3\bar{\gamma}}{\mu r} t$ where $\bar{\gamma}$ is the contact-area-weighted average tension, and r is the average cell radius [19].

of closed loops is quite different. Some of these loops seal off [loop **P** in Figs. 2(a) and 2(b)] and others break open [loop **Q** in Figs. 2(a) and 2(c)]. These two processes untangle the two cell domains and are duals of one another—breaking a connected chain of either minority or majority cells. As the boundary around the minority cells then continues to contract, it draws the minority cells together into a compact, slightly nonspherical mass. Sorting in this case breaks some favorable cell-cell attachments, but no fluctuations are necessary.

Such chain breakage is possible in 3D by a process analogous to the Plateau-Rayleigh instability. This instability is driven by surface tension, breaks thin fluid streams into droplets [21], and plays an important role in the phase separation of immiscible fluids [22]. With a strong analogy to phase separation [23], a similar role is expected in cell sorting. There is some limited evidence for this instability in real cells [24], and finite-element simulations of thin chains of cells [Fig. 3(a) and Movie 2, see supplementary material [20]] show that these structures do spontaneously neck and pinch off (when length > diameter). Note that this instability does not occur in 2D, including cell-sorting experiments [5], models [6,17], and immiscible fluids [25]. As a result, 2D cell chains are durable in the absence of fluctuations and keep islands of minority cells isolated from each other [5,6].

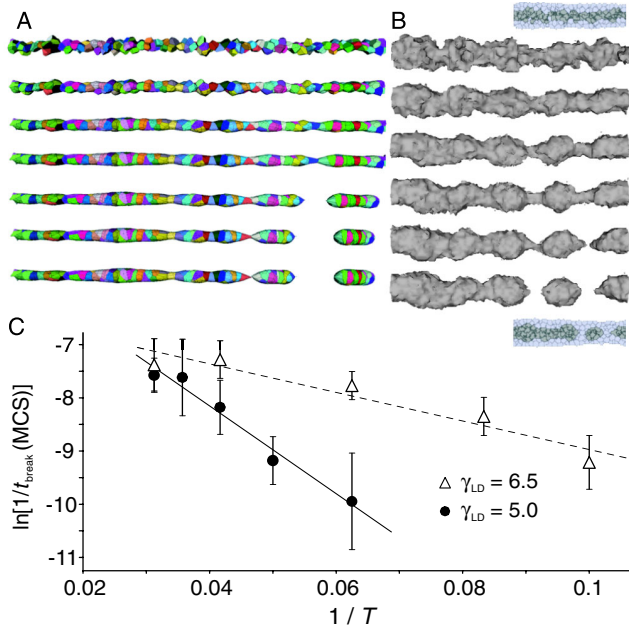


FIG. 3 (color online). Plateau-Rayleigh instabilities in thin rods of cells: (a) finite-element model and (b) cellular Potts model. Time advances down each column with breakage occurring at $\tau = 78$ (a) or $t = 2510$ MCS (b). In (b), the outer sheath of cells (light gray) is only shown in the early and late time insets. (c) Arrhenius plot showing how the rate of rod breakage depends on the Potts model temperature. Each point is the average of five simulations. The lines are the best linear fits.

Such instabilities should also occur in other 3D models, so we ran simulations of thin chains of cells using a cellular Potts model. When the contact surface energies are set to match those used in previous cell-sorting simulations ($\gamma_{LL}:\gamma_{DD}:\gamma_{LD}:\gamma_{L0}:\gamma_{D0} = 7:2:5:8:8$ which yields $\sigma_L:\sigma_{LD}:\sigma_D = 4.5:0.5:7$) [13,14], chains of dark cells enclosed in a sheath of light cells do break at high temperatures ($T \geq 16$), but they break and reform multiple times. When γ_{LD} is increased to 6.5 (so $\sigma_{LD} = 2.0$), the higher heterotypic tension allows the chains to irreversibly break at lower temperatures [Fig. 3(b)]. In both cases, the rate of chain breakage is strongly dependent on the simulated temperature. This dependence is shown on the Arrhenius plot in Fig. 3(c) where linear regression yields a higher activation energy barrier for low γ_{LD} (82.5 ± 7.8) than for high (26.9 ± 4.6). These activation barriers to chain breakage are artificial. They are introduced by the way Potts models drive cell motion, i.e., through the accumulation of “spin” flips at single lattice sites. When collective motions are handled exactly, as in the finite-element model, interfacial tension drives chain breakage with no activation barrier.

The above results suggest that heterotypic interfacial tension should have a profound effect on 3D cell sorting, especially when the initial configuration has entangled co-continuous domains. To confirm, we ran sorting simulations of 670 cells with both models, at two different

minority-cell fractions ($f = 15$ and 30%) and either high or low tension ($\gamma_{LD} = 6.5$ or 5 as above). For the Potts model, the average cell size was 97 lattice sites. We also used three different temperatures ($T = 4, 12$, and 32).

We evaluated sorting with four metrics (Fig. 4): the contact areas (A_{D0} , A_{LD} , normalized by the total cell-medium contact area, $\sim 4\pi R^2$ where R is the equivalent aggregate radius); the minority-cell Euler characteristic (χ_D); and the density correlation length (L , normalized by the value expected for a uniform sphere of the same volume, $\frac{36}{35}R$) [4]. These metrics report on different aspects of sorting and together build a complete and consistent story.

For the Potts model, sorting is always complete at high T and incomplete at low T . In either case, some metrics approach their fully sorted value faster at low heterotypic tension: A_{D0} which reports on surface clearance, and χ_D at $f = 15\%$ which reports on domain coalescence. Other metrics change faster at high tension: A_{LD} and χ_D at $f = 30\%$ which mainly report on untangling. The data for χ_D at $f = 30\%$ also contains instructive subtleties that highlight the dual role of γ_{LD} . At all T , high tension causes faster

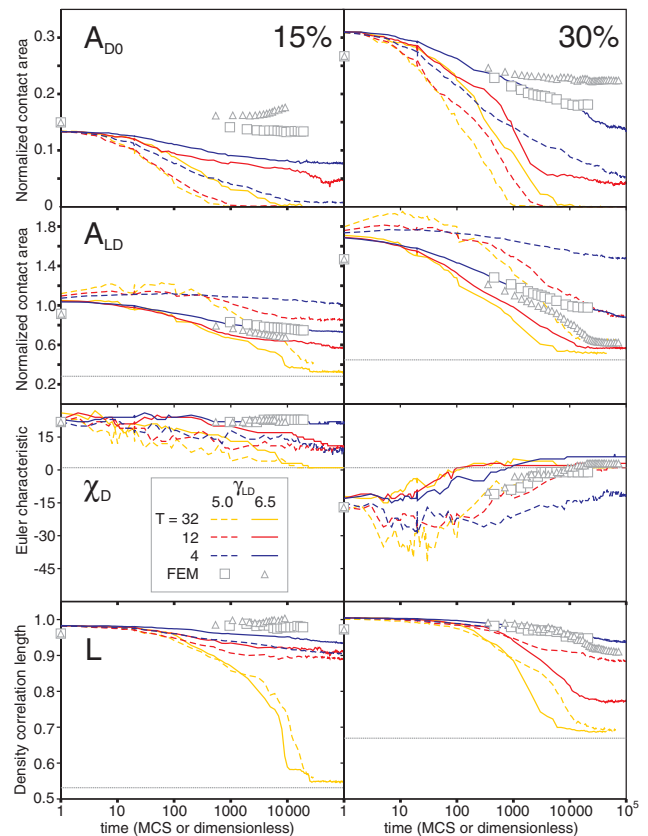


FIG. 4 (color online). Dependence of sorting metrics on fluctuations and heterotypic interfacial tension. The target value for each metric after complete sorting is shown with thin gray lines (except A_{D0} where the target value is zero). The finite-element simulations were stopped when sorting stopped. Each model’s results are plotted using its own time axis (MCS or dimensionless time).

increases in χ_D , but it also causes χ_D to overshoot its target value of one. After the overshoot, only the high T data eventually returns to one. Such overshoots do not occur at low tension and only occur when the rate of untangling is much faster than the rate of domain coalescence. The final metric, the density correlation length, also depends on multiple aspects of sorting. When coalescence dominates, L decreases faster at low tension—the opposite when untangling dominates.

Although the Potts models require fluctuations to achieve any degree of sorting, the finite-element models can achieve partial sorting with completely deterministic motions. The degree of deterministic sorting is much larger when sorting is dominated by domain untangling (i.e., $f = 30\%$). When this partial sorting does occur, the heterotypic interfacial tension impacts the sorting metrics in the same way as in the Potts models. It slightly slows the decrease of A_{DO} , speeds the decrease of A_{LD} , and brings χ_D and L closer to their target values. On the other hand, the finite-element models produce very little sorting when domain coalescence dominates ($f = 15\%$). Preliminary investigations show that partial coalescence can occur when fluctuations are added.

Taken together, the two models show that 3D cell sorting has to be considered as three overlapping processes: (1) clearance of dark cells from the aggregate surface, (2) domain coalescence, and (3) domain untangling. The first two require fluctuations and are inhibited by high tension at heterotypic interfaces. The third does not require fluctuations and is actually driven by γ_{LD} (through a Plateau-Rayleigh instability). In 2D, domain coalescence and untangling cannot be separated, and the Plateau-Rayleigh instability does not occur.

These processes impact the sorting kinetics differently as the minority-cell fraction changes—which points to feasible, yet stringent, experimental tests. Previous studies each reported the kinetics for a single f , but the models can fit this data with multiple parameter sets, each using a different temporal scale factor. For example, the $f = 15\%$ data from [14] can be fit by the high- T Potts model with high or low γ_{LD} at 30 or 15 s per Monte Carlo step (MCS), respectively. Similarly, the $f = 50\%$ data from [4] (which used different cell types) can be fit with the Potts model, but with very different scaling factors—3.7 or 0.44 s per MCS [20]. The finite-element model also fits this data (up until sorting halts in the model without fluctuations) using high γ_{LD} and a scale of 0.07 s per unit. A more stringent test would be to measure the 3D sorting kinetics for $f = 10\text{--}50\%$ with a single pair of cell types. If correct, a model should reproduce the kinetics for all f with a single parameter set and temporal scale. Such tests

could be extended by adding cytochalasin D to suppress active cell fluctuations [14], which is predicted to halt sorting early at $f < 15\%$, but much later at $f > 30\%$. These two experiments would very effectively test whether the models properly balance the roles identified here for fluctuation-driven and surface-tension-driven kinetics.

This work was supported by the Natural Sciences and Engineering Research Council of Canada (G. W. B., D. V., J. Y.), by the National Science Foundation (M. S. H.), and by the Human Frontier Science Program (G. W. B., M. S. H.).

*Corresponding authors: shane.hutson@vanderbilt.edu, brodland@uwaterloo.ca

- [1] P. B. Armstrong, Crit. Rev. Biochem. Mol. Biol. **24**, 119 (1989).
- [2] M. S. Steinberg, Science **137**, 762 (1962).
- [3] M. S. Steinberg, Dev. Biol. **180**, 377 (1996).
- [4] N. Kataoka, K. Saito, and Y. Sawada, Phys. Rev. Lett. **82**, 1075 (1999).
- [5] C. B. Collares-Buzato *et al.*, Cell Tissue Res. **291**, 267 (1998).
- [6] G. W. Brodland, Appl. Mech. Rev. **57**, 47 (2004).
- [7] M. S. Steinberg, J. Exp. Zool. **173**, 395 (1970).
- [8] F. Graner, J. Theor. Biol. **164**, 455 (1993).
- [9] R. A. Foty *et al.*, Phys. Rev. Lett. **72**, 2298 (1994).
- [10] J. A. Glazier and F. Graner, Phys. Rev. E **47**, 2128 (1993).
- [11] H. Honda, M. Tanemura, and T. Nagai, J. Theor. Biol. **226**, 439 (2004).
- [12] E. Palsson, Future Gener. Comput. Syst. **17**, 835 (2001).
- [13] J. A. Glazier *et al.*, in *Interplay of Genetic and Physical Processes in the Development of Biological Form*, edited by D. Beysens, G. Forgacs, and F. Gaill (World Scientific, Singapore, 1995), p. 54.
- [14] J. C. M. Mombach *et al.*, Phys. Rev. Lett. **75**, 2244 (1995).
- [15] J. C. M. Mombach, Phys. Rev. E **59**, R3827 (1999).
- [16] C.-N. Lee, T. Poston, and A. Rosenfeld, CVGIP: Graphical Models and Image Processing **53**, 522 (1991).
- [17] G. W. Brodland, J. Biomech. Eng. **124**, 188 (2002).
- [18] T. Lecuit and P. F. Lenne, Nat. Rev. Mol. Cell Biol. **8**, 633 (2007).
- [19] D. Viens and G. W. Brodland, J. Biomech. Eng. **129**, 651 (2007).
- [20] See EPAPS Document No. E-PRLTAO-101-073840 for movies and graphs of model fits. For more information on EPAPS, see <http://www.aip.org/pubservs/epaps.html>.
- [21] S. Tomotika, Proc. R. Soc. A **150**, 322 (1935).
- [22] E. D. Siggia, Phys. Rev. A **20**, 595 (1979).
- [23] D. A. Beysens, G. Forgacs, and J. A. Glazier, Proc. Natl. Acad. Sci. U.S.A. **97**, 9467 (2000).
- [24] R. Gordon *et al.*, J. Theor. Biol. **37**, 43 (1972).
- [25] Y. Son *et al.*, Macromolecules **36**, 5825 (2003).